ISSN 0016-8521, Geotectonics, 2024, Vol. 58, No. 1, pp. 23–40. © Pleiades Publishing, Ltd., 2024.

Arc Tectonic Elements and Upper Mantle Structure of Central and Southeast Asia: Seismic Tomography and Seismicity Data

S. Yu. Sokolov[a], * and V. G. Trifonov[a]

[a] *Geological Institute, Russian Academy of Sciences, Moscow, 119017 Russia*

**e-mail: sysokolov@yandex.ru*

Received November 27, 2023; revised February 23, 2024; accepted February 29, 2024

Abstract—Analysis of the upper mantle plumes spatial distribution in the inner part of the Sunda arc shows a number of plume bodies interrupting the stagnant slab framed from the south by the sinking slab of the Sunda arc. Possible mechanisms resulting in this structure of the mantle are (i) W-E-trending toroidal mantle flow through a gap in a flat slab and (ii) rollback capable of forming a gap in a flat slab and launching upper mantle plumes in it without deep (>1000 km) roots. The space above the top of the slab consists of local hot mantle bodies, which are considered secondary plumes and often form local rift segments. The 3D visualization of velocity variations δV_p in the Tibet and Central Asia region demonstrates structural patterns similar to those in the Sunda arc area. One can observe a region of subhorizontal slab fragments and a gap, which is recorded by plume anomalies of deep and secondary origin. The motion vectors of the rock mass along the fault planes of the Sunda arc, detected from seismic events, are directed outward from its center of curvature, in which secondary upper mantle plumes are concentrated. This indicates the development of thrust processes at the arc front unassociated with the subducting plate. The arc thrusting is accompanied by a small number of displacements along antithetic thrust faults. The displacement azimuths along the Himalayas are fan-shaped, oriented toward Hindustan. This shows that the main indicator of tectonic activity (seismic events) has a direction of rock mass displacement to the south from the extensional back-arc basin within Tibet with the development of thrust deformations during movements along the detachment planes. Two directions of seismic movements are distinguished in the Himalayan arc, as well as in the Sunda arc. The first direction follows the Indian Plate subduction model. The second direction includes variable azimuth rock mass movements along the thrust planes onto the Indian Plate.

Keywords: Himalayas, Sunda arc, Indian Plate, directions of rock mass displacement, focal seismic mechanisms, mantle plumes, plate thrusting

DOI: 10.1134/S001685212470002X

INTRODUCTION

The application of seismotomography to studying velocity heterogeneities in the mantle made it possible to detect high-velocity "cold" anomalies"—slabs that extend from subduction zones to depths of up to 2000 km. This is one of the most important recent geological discoveries. A review of these anomalies is given in [29]. It was also shown that in some cases, slabs are gradually flattened and lie horizontally in the depth range of 410–660 km. Due to this, there are many uncertainties in understanding the origin and structure of real mantle convection [29].

Thirty-six regional seismotomographic sections across convergent ocean boundaries have been calculated for subduction zones of the Northwest Pacific Rim. In addition, it has been established that the slab geometry with flattening in the above depth range predominates [5]. A special term—stagnant slabs—has been proposed for this configuration of mantle heterogeneities. They have also been identified in the Alpine–Himalayan–Indonesian belt [12].

Analysis of the velocity field of horizontal movements of the main lithospheric plates in the NNR (no network rotation) reference frame [18] shows that the continental plates beneath which the oceanic plates are subducting show reverse directions of motion toward the ocean. In our opinion, this indicates the necessity of thrust processes in the subduction zones.

As defined in [2], the convergent movement of the Eurasian Plate and Indian microcontinent creates the condition for the formation of stagnant blocks and initiation of the rollback mechanism [6]. During the latter, separate convection unconnected with the rest of the mantle operates in a depth interval of <660 km, and back-arc rift structures are formed with shallow secondary plumes and volcanism. These back-arc structures in the seismotomographic field represent low-velocity "hot" anomalies, which caused the breakup of "cold" stagnant slabs [5, 35].

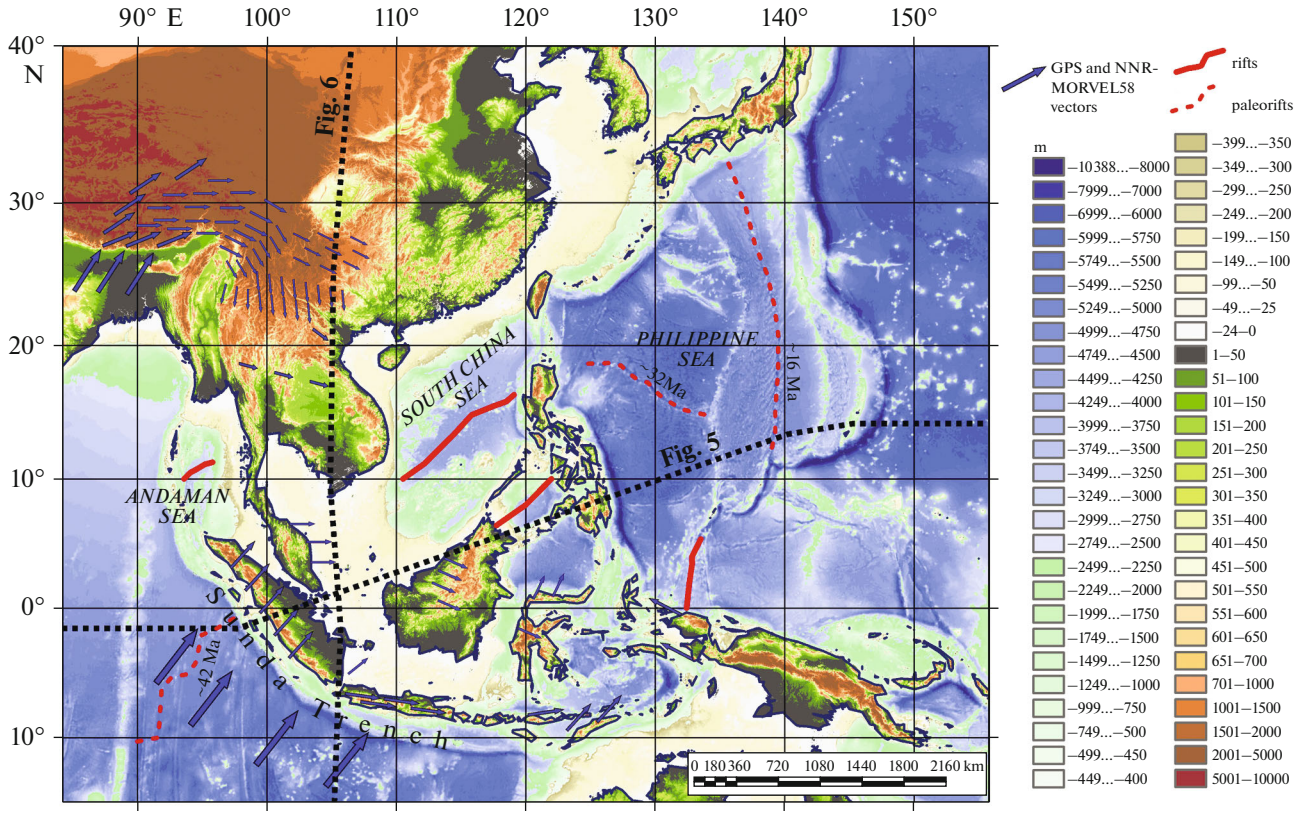

Fig. 1. Scheme of horizontal motion of lithospheric plates and blocks in Southeast Asia, continental China, India, and Indonesia (after [18, 33, 34, 38, 39]). Scheme is constructed for continental part of China and India based on GPS data from [34, 38]; for Indonesia, based on GPS data from [33]. Scheme of Australian plate movement is constructed based on NNR-MORVEL56 model [18].

This combination of geodynamically active lithosphere blocks is manifested not only at the continent–ocean boundary, but also in Central Asia where Hindustan collides with the Eurasian continent (Fig. 1).

As follows from the peculiarities of the horizontal motion vector fields obtained from GPS data, this gives further scope for different interpretations of what kinds of mechanisms occur in reality [18, 33, 38]. In particular, approximation of plate kinematics by a single value of the pole and rotational rate for the whole plate contradicts real GPS data [18, 33, 38], which may differ by 180° from the plate-average values. This problem is solved by the method of the breaking plates into smaller parts [18], which is quite justified for describing the tectonic motion kinematics, but it does not explain the geodynamic mechanism.

In [23], the model field of plate rates was compared with GPS measurements and it was shown that the maximum divergence between these kinematic parameters occurs in structural arcs. This may indicate that calculating the rate when determining the models does not include the processes taking place in reality.

In our opinion, in addition to GPS vectors, there is a type of data that can also contribute to solving the problem, but it is usually not represented in kinematic schemes. These data represent the orientation of strong earthquake slip vectors along fault planes according to the CMT catalog [24], which differ from the GPS vector field (Fig. 2).

The present paper aims at comparing variations in seismic wave velocities in the mantle in the back-arc part of Central Asia with those in Southeast Asia, chosen as a reference region of this geodynamic setting, as well as the modern kinematics of arc structures taking into account earthquake slip vectors.

TECTONIC SETTING

A series of extended tectonic zones are distinguished in and to the north of the Central Asian segment of the Alpine–Himalayan mobile belt. It represents alternating noncoeval fold–thrust zones with blocks where the ancient crystalline basement is exposed or overlain by a relatively weakly deformed sedimentary cover.

Fold–Thrust Zones

North of the Himalayan flank of the Indian Platform, between the Pamir–Punjab Syntaxis and eastern ends of the Himalayas and Tibet, the following

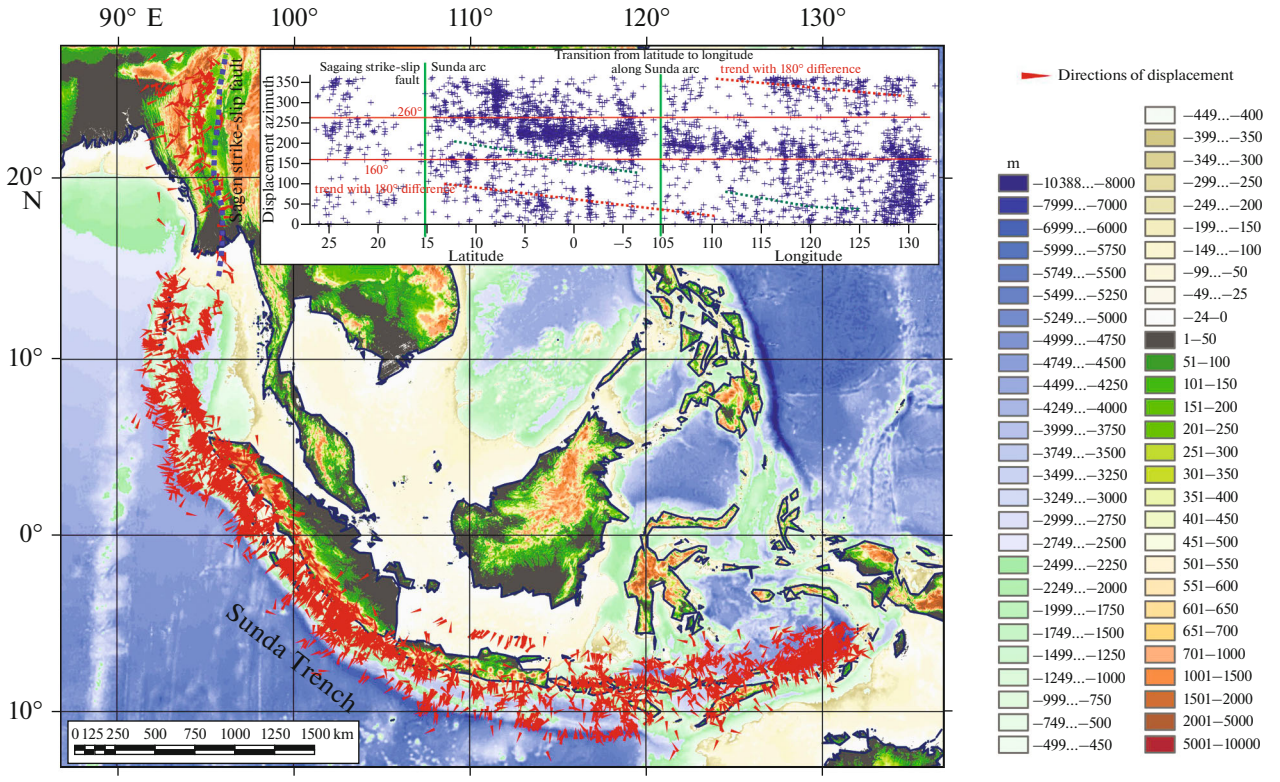

Fig. 2. Azimuths of rock mass displacements along strong earthquake fault planes according to CMT catalog [24, 39]. Inset: cluster of displacement azimuth points along Sunda trench and Sagaing dextral strike-slip fault.

structures are distinguished from south to north [4, 13] (Fig. 3).

— The Cis-Himalayan trough that is deformed on the northern flank.

— The Himalayan neotectonic uplift—the Precambrian basement of the Indian Platform, overlain locally by the Gondwanan Platform cover. To the north, the cover assumes the features of the Neotethys passive margin. The Main Central Thrust (MCT), Main Boundary Thrust (MBT), and Main Frontal Thrust (MFT) are evidence of thrusting of the Himalayan mountain system on the Indian Platform or subduction of the platform beneath the Himalayas.

— The Kohistan and Ladakh zone—a Neotethys volcanic arc with large granitic batholiths. The basement of the arc (ultramafic rocks and granulites; higher in the succession, amphibolites and gabbronorites) crops out in the zone of the Main Mantle Thrust (MMT), which bounds this zone from the south. In Tibet, this zone corresponds to the southern part of the Lhasa block and the Indus–Tsangpo zone (Neotethys suture). The Paleocene and Eocene ophiolitic and island-arc elements are tectonically juxtaposed in this zone. They are highly deformed and unconformably overlain by Oligocene–Miocene conglomerates [16].

— The southern part of the Karakorum and eastern Hindu Kush with intensive regional metamorphism and the emplacement of the axial batholith, bounded from the Main Karakorum Thrust on the south. The Shyok suture with an ophiolite melange is distinguished in the zone of this thrust. It marks the Late Mesotethys basin, which closed in the Middle Cretaceous, or the Neotethys back-arc basin [30]. The rocks near the suture zone were deformed in the Cenomanian–Turonian. In Tibet, the Shyok suture is followed by the Bangong suture, which marks the development of the Late Triassic–Jurassic basin, which was terminated by collision in the Middle Cretaceous [4]. The ophiolites are obducted onto the Lhasa Block.

— The Northern Karakoram Zone with the Cambrian–Proterozoic continental basement [21]. In the Pamir–Punjab Syntaxis, this zone passes northward into the Southeast Pamir and Nuristan, where carbonate platform facies are followed northward by relatively deep-water flyschoid slope facies of the Early Mesotethys basin.

— The Pshart suture in the Pamir is a relict fragment of the Early Mesotethys. The Upper Permian–Triassic strata of the latter are unconformably overlain by Namurian volcanoterrigenous deposits. We consider the Ulan Ula and Yushu ophiolite zones in Eastern Tibet—traces of an oceanic basin that closed no later than the Early Triassic—to be the eastern contin-

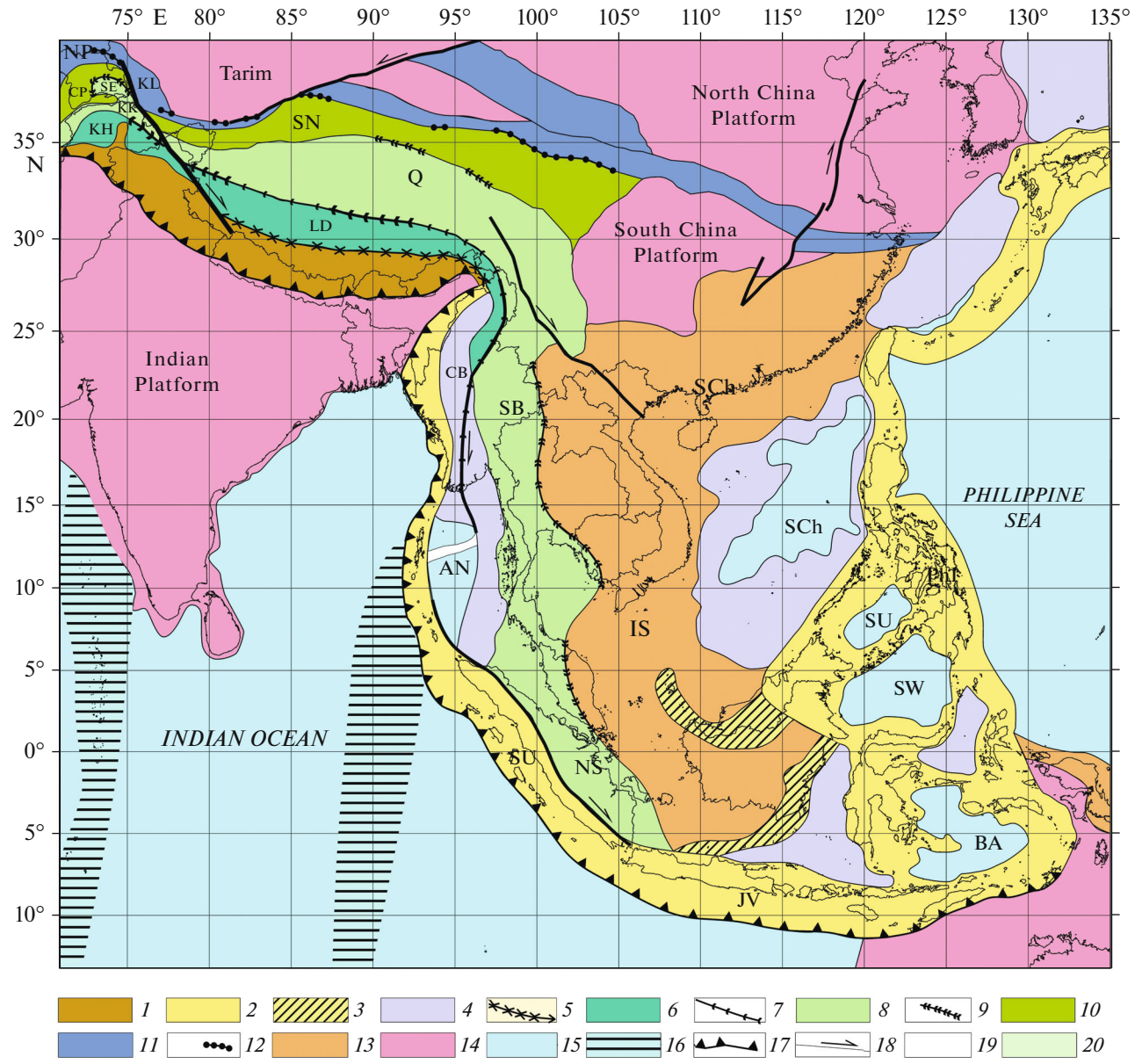

Fig. 3. Tectonic map of major structures of Himalayan–Tibet region and SoutheastAsia (after [3, 4, 13–15]). *Modern island arcs*: SU, Sunda; Phi, Philippine; JV, Java; *Seas*: AN, Andaman; BA, Banda; SW, Sulawesi; SL, Sulu; SCh, South China; *Trough*: CB, Central Burma; *Zone*: ITs, Indo–Tsangpo; *Northern active margin of Neotethys*: KH, Kohistan; LD, Lhasa; *Southern passive margin of early Mesotethys*: KK, Northern Karakoram; SE, Nuristan and Southeastern Pamir; Q, Qiantang; SB, Sino-Burma Massif; NS, Northeastern Sumatra; *Northern margin of early Mesotethys*: CP, Central and Southwestern Pamir; SN, Sunpan; *Late Hercynides*: NP, Northern Pamir; KL, Kunlun; *Paleozoids*: SCh, Southeastern China; IS, Indosinian Massif; (*1*) Himalayan neotectonic uplift; (*2*) modern island arcs (from base of arc slope of a trench to volcanic arc inclusive); (*3*) island arcs; (*4*) modern back-arc basins (northern continuation of Andaman Sea covered by fluvial sediments); (*5*) Neotethys suture; (*6*) northern active margin of Neotethys; (*7*) suture zone of Late Mesotethys or Neotethys back-arc sea; (*8*) southern passive margin of Early Mesotethys; (*9*) suture zone of Early Mesotethys; (*10*) northern margin of Early Mesotethys; (*11*) Late Hercynides; (*12*) Late Paleozoic sutures; (*13*) Paleozoides; (*14*) Precambrian platforms and microplates with Precambrian basement in Paleozoic fold belts; (*15*) oceanic crust areas; (*16*) 70° and 90° E rises in Indian Ocean; (*17*) largest modern thrusts and underthrusts in frontal parts of island arcs and Himalayas; (*18*) largest modern strike-slip faults; (*19*) rift zones in Andaman Sea; (*20*) boundary areas of tectonic provinces and zones.

uation of the Pshart suture. Under such a comparison, the Southeastern Pamir and Northern Karakoram correspond to the Qiantang zone in Tibet, and the Songpan Zone corresponds to the Central Pamir.

A number of Paleozoic tectonic zones are distinguished further to the north, which are separated by Precambrian blocks that have experienced tectonomagmatic reworking to a greater or lesser extent [8].

In the south, these are Middle and Late Paleozoic linear fold–thrust zones. As a rule, the more northern the location of the zones, the older their age is. The southernmost zone is the Northern Pamir–Northern Kunlun, formed in the Late Paleozoic [4].

Eastwardly, the Qaidam and the folded mountain chain separating the North and South China Precambrian platforms probably belong to this zone. The youngest fold–thrust deformations occurred in these parts of the zone in the Late Paleozoic and, in some places, in the Triassic.

The Solonker fold–thrust zone, distinguished in Southern Mongolia, and the Mongolian–Okhotsk relics occupy a special place in the northern part of Central Asia. The strata of the Solonker Zone with Visean–Early Permian ophiolites experienced fold–thrust deformations in the Middle Triassic. The development of the western Mongolian–Okhotsk Ocean terminated with collision in the Jurassic and, in some places, in the Lower Cretaceous [3, 9].

The Solonker Zone forms the northern boundary of the Katasian microcontinent, which hosts the Precambrian North and South China platforms and Paleozoides of Southeast China.

In the east, the tectonic zones of Tibet curve southward and continue into Indochina along the eastern margin of the Indian Ocean [3, 15] (Fig. 3). The Bangong suture zone extends along the Sagaing dextral strike-slip fault to the mouth of the Irrawaddy River. The Indosinian suture, which continues the Early Mesotethys suture marked by Ulan Ula and Yushu ophiolites, reaches the Malacca Peninsula across the Yunnan Ridge, northwestern Laos, Thailand, and western Cambodia. In this zone, the ophiolites are exposed among Triassic–Upper Paleozoic volcanosedimentary rocks, which formed in the central part and on the walls of the deep-water basin. Its closure at the end of the Triassic was accompanied by intense fold–thrust deformations.

The fold complexes are unconformably overlain by Norian–Jurassic red deposits. The Sino-Birma Massif is located between the continuation of the Bangong and Indosinian suture zones. The Indosinian massif is located to the east of the eponymous suture. Further east, the latter passes into the Paleozoides in Southeast China.

Southwestern Kalimantan is located to the south, which extends toward the southern shelf of the South China Sea and probably the Java Sea. In southwest Kalimantan, crystalline schists are overlain by Upper Paleozoic and Jurassic–Cretaceous shallow deposits and intruded by Upper Jurassic and Cretaceous granitoids.

The Mesozoic and older tectonic zones of Indochina and the Indonesian–Philippine Archipelago were subject to essential reworking in the Cenozoic. The Sunda arc extends in the west and south of the region. In the north, in the Myanma segment, the arc is presented by a series of the Indo-Burma fold–thrust belts, which is an accretionary wedge over the east-dipping subduction zone of the Indian Plate. The belts are composed of Upper Cretaceous and Paleogene rocks deformed in the Late Oligocene. East of the arc is the Central Burma Depression with several-kilometer-thick Cenozoic molasse strata.

The Indo-Burma belts are traced southward as a chain of the Andaman–Nicobar Islands, which form the nonvolcanic part of the arc. Its volcanic part is represented by predominantly andesitic rocks at the boundary of the islands with the back-arc Andaman Sea. In the central part of the sea, where the Earth's crust is close to the oceanic type, a rift zone, established 10.8 Ma ago, was identified [15]. The rifts are combined with transform faults. The eastern fault passes into the Sagaing strike-slip fault, while the western fault is continued by the Central Sumatra dextral strike-slip fault. Thus, the Andaman Sea is a pull-apart trough.

The volcanic arc is traced on Sumatra, Java, and the more eastern islands. In Java, volcanism began in the Middle Miocene. In the eastern segment of the arc, south of the Banda Sea, the submarine continental margin of Australia approaches it. The island of Timor is in the structure of the arc, where the continental crust has a thickness of 60 km and Pliocene corals are elevated to a height of 800 m [15].

The maximum depth of earthquake sources increases to southeast as follows [24]:

— 150 km beneath Burma;

— 200 km beneath the Andaman–Nicobar Islands;

— >300 km beneath Sumatra;

— 600 km beneath Java.

The depth of the trough increases from 4 to 8 km in the same direction.

In the east, the study area is bounded by the Marianan arc with the Philippinian back-arc sea. Closer to the center, the Philippine island arc is located over the west-dipping subduction zone of the oceanic lithosphere. The territory between the Philippine and Sunda arcs is heterogeneous. Along with fragments of continental blocks, ophiolites, volcanic arcs and deep-water depressions of different Cenozoic epochs have been identified here.

In northern Kalimantan, an accretionary wedge with Cretaceous–Paleogene flysch was distinguished, which is conjugate with a magmatic arc located to the south and formed over the south-dipping subduction zone of the oceanic lithosphere. This wedge was dislocated in the Late Eocene during collision with the continent to the north.

In northeast Kalimantan, there is a Miocene volcanic arc underlain by Cretaceous ophiolites. It joins the Philippines to the east and separates the Sulawesi and Sulu seas. The Sulawesi and Banda Seas are surrounded by ophiolites and volcanic arcs on almost all

sides. The Sulu, Sulawesi and Banda sea basins are characterized by an oceanic type of crust.

MATERIAL AND METHODS

The UU-P07 seismotomographic model [16, 17, 36], calculated from teleseismic data with a spatial resolution of ~100 km in seismically active zones, was chosen to analyze seismic *P*-wave velocity variations (δV_p). A specific feature of this model is 3D initial approximation, starting from which velocity variations are calculated to adapt to recroded seismic signals.

For a long time, the radially symmetric preliminary reference Earth model (PREM) was used as the initial approximation [31].

In the 2000s, many models calculated at low-frequency spherical harmonics up to $l = 20$ became very similar [19]. This led to the idea of introducing 3D initial approximations [17], which vastly improved the quality of δV_p calculations and the computational result of the used algorithms.

We applied the UU-P07 model to construct velocity sections of the mantle along profiles with an arbitrarily defined trajectory on a surface that is not on the arc of a great circle between two points on a sphere. The UU-P07 model was also used for volumetric mapping of mantle structures in the studied regions by combining orthogonal cross sections of the mantle with focus on key objects and filling of the space between cross sections with a partially transparent isosurface having specified δV_p values. This combination of volumetric elements allows us to show volumetric inhomogeneities in a rather informative way.

We used seismic data to obtain information on the orientation of strong earthquake slip vectors along fault planes and plot the spatial distribution of these vectors along arc areas based on the CMT catalog data [24].

The traditional representation of earthquake focal mechanisms adequately shows the kinematic type of seismic events, but the peculiarities of strong earthquake slip vectors along fault planes are not expressed in such a way as to make them fully perceptible.

The CMT catalog [24] contains information about the strike, dip angle of a fault plane, and displacement angle along this plane, according to the reference system [1] determined from the counterclockwise azimuth.

Data of these parameters in the CMT catalog [24] are presented for two fault planes: main and auxiliary. The difference between the displacement azimuths along these planes, calculated as the difference between the fault-plane azimuth angle and displacement angle and projected on the surface, is 180°.

The directions for the auxiliary plane have a physically unrealizable orientation. According to the latter, vectors along the Sunda arc, converging to its center of curvature, and a common displacement azimuth of the subducting Indian Plate, constant along the entire length of the arc, occur simultaneously.

Therefore, to analyze the directions of rock mass displacement during the motion of the crustal and upper mantle block, we compiled displacement maps along the main plane and compared them with mantle velocity anomalies δV_p.

ANALYSIS

Seismotomographic Data

In the visualization of δV_p velocity variations, the spatial distribution of slabs around the Sunda Trench and the bark-arc area within the plane table boundaries (Fig. 1) is as follows (Fig. 4).

The cold slab bodies displayed from the viewpoint above and along the 0.33% isosurface to the south have maximum lateral distribution at depths of ~950 km. Deeper, the isosurface turns beneath the slab and is not displayed from a single viewpoint. In the bark-arc area, the slab is gradually flattened and obtains a so-called stagnant configuration. Smaller fragments of solid bodies are distinguished beneath the northern segment of the Andaman arc throughout the depth of their maximum distribution up to a depth of 950 km. The stagnant branch at a depth of the transitional mantle layer detaches from the slab. The cold slab body was recorded beneath the Philippine arc, where it amalgamates at the level of the transition layer with an extensive subhorizontal cold lens, and the Mariana arc at a depth of up to 670 km.

The hot mantle bodies have been identified in the Andaman back arc and beneath the Philippines. At a mantle section at a depth of 950 km, the cold body extends along the Indonesian part of the arc and is interrupted by hot anomalies of South China, Philippines, and Andaman seas.

The latitudinal mantle section crossing all arcs in the area under consideration shows that the hottest bodies occur 400 km above the upper mantle beneath the Southern Philippines and the adjacent sea from the west to North Kalimantan, as well as immediately in the back-arc part of the Andaman arc. Hot bodies were recorded at the following locations (Fig. 5).

Hot bodies:

— in front of the Sunda Trough (the body is dipping westward from the trough beneath the Ninety East Ridge from the upper mantle to ~800 km);

— at depths up to 500 km from the Andaman arc to the Philippines and the westernmost part of the Philippine Sea.

"Cold" bodies:

— a subhorizontal cold lens at depths from 700–800 km (800 km in the west and 700 km in the east) to 1200–1500 km (the maximum depth of the lens bottom is under the marginal sea west of the Philippines, the lens extends from the Andaman arc to the western

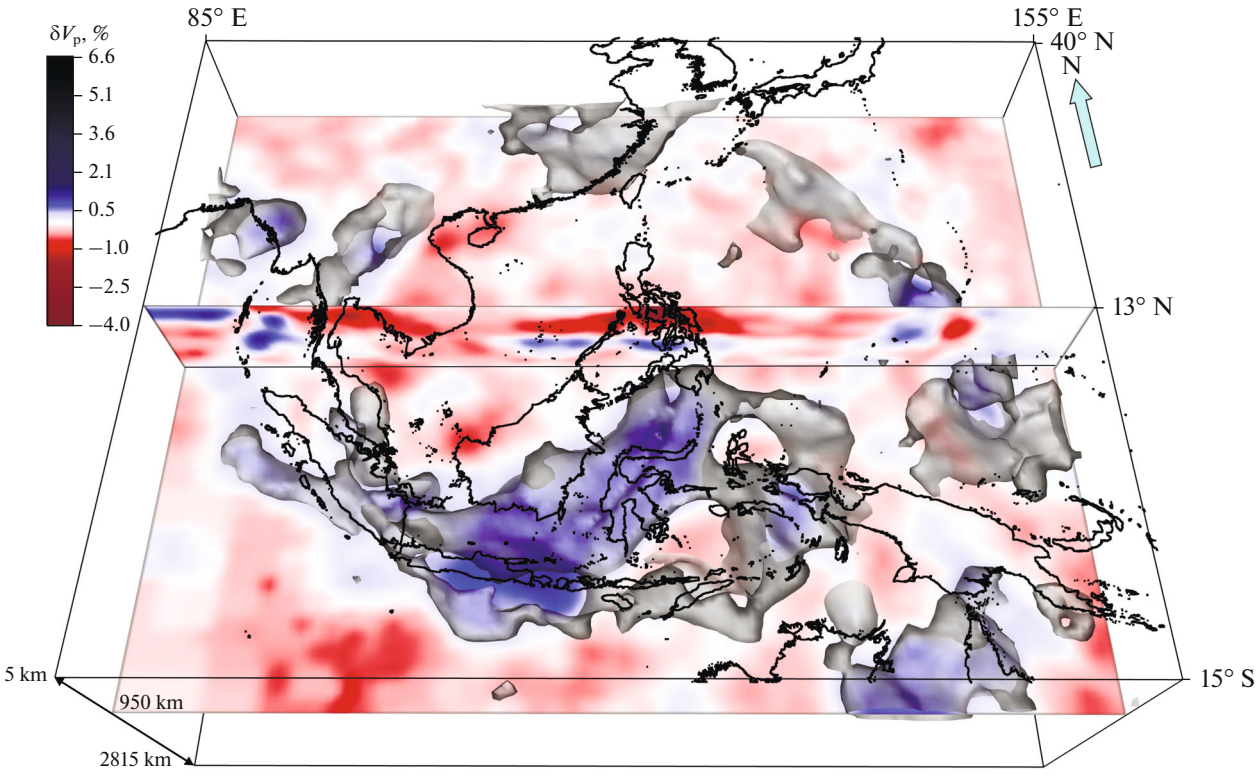

Fig. 4. 3D visualization of δV_p velocity variations in Southeast Asia according to UU-P07 model [17, 26, 36]. Viewpoint is located in south and oriented to depth from surface. Isosurface is shown for positive variation values of 0.33% with partial transparency.

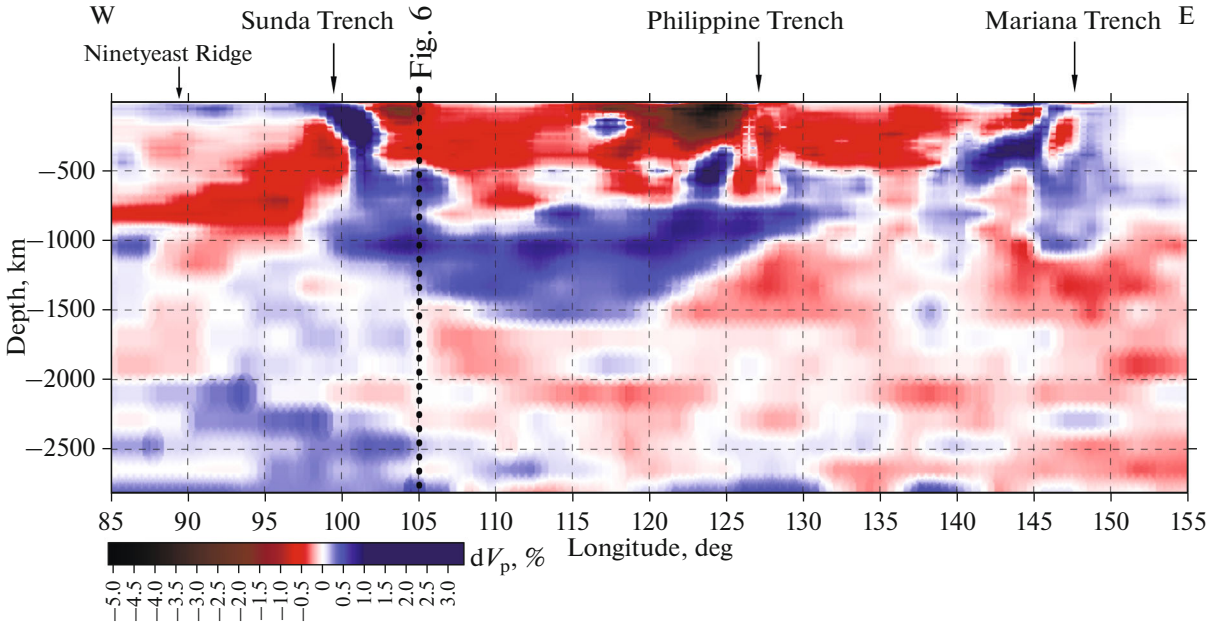

Fig. 5. Seismotomographic section along sublatitudinal profile according to UU-P07 model [17, 26, 36]. For position of profile see Fig. 1; intersection with section (dashed line) is shown in Fig. 6.

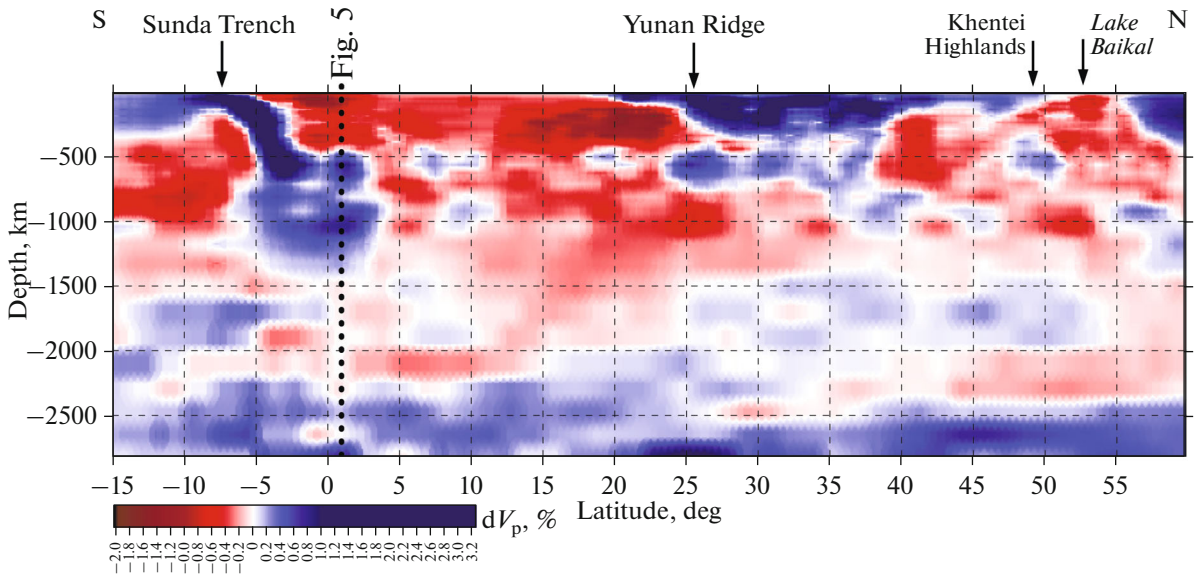

Fig. 6. Seismotomographic section along sublongitudinal profile based on UU-P07 model [17, 26, 36]. For position of profile see Fig. 1; intersection with section (dashed line) is shown in Fig. 5.

edge of the Philippine Sea, the highest velocities are characteristic of the upper part of the lens);

— the Andaman slab with a stagnant branch bounded in extent (<3°) at the level of the transition layer; the slab is traced to a depth of 800 km up to the cold lens (Figs. 4, 5);

— the Philippine slab, which is most distinctly expressed at depths of 300–700 km, connects with a lens at a depth of 750 km;

— the Mariana slab, which is most distinctly expressed at depths of 200–600 km, connects with a lens at a depth of 700 km.

The cold bodies, which occur inside the Sunda arc, on the submeridional section look the same as on the sublatitudinal section. However, the gap in the slab, through which hot plume bodies rise to the surface, is clearly visible (Figs. 5, 6).

North of the arc, the upper mantle, hot to a depth of up to 500 km, can be traced to the Yunnan Ridge. The upper mantle to the east of the Andaman arc and beneath the East Tibet is considered the hottest. The hot mantle volume can be traced beneath Tibet to a depth of at least 1200 km.

At the level of the transition layer of the mantle relatively small lenses of cold mantle are distinguished. Further to the north, the upper mantle is traced to a depth of up to 350 km. The hot mantle of the Khangai plume branches appears near the Khentei Plateau and continues northward towards Transbaikalia [14].

The region eastward of the Sunda Trench is the most pronounced structural ensemble, which comprises slab-type mantle anomalies, including the stagnant ones, plume-type hot anomalies, a break in the slab with penetration of hot bodies to bark-arc areas of extension and modern rifting. This area can be considered as a geodynamic benchmark combining all the above structures.

In 3D visualization of δV_p velocity variations, the spatial distribution of slabs in the Tibet–Himalayan region and the Central Asia within the boundaries of the studied area is shown in Fig. 7.

The cold slab flat-topped bodies, recorded from the viewpoint above and to the southeast at 0.33% isosurface, have a lateral distribution at depths up to ~1000 km, similar to the Sunda back-arc area. The vast area of subhorizontal slabs north of Tibet has a gap through which plume anomalies rise. Further to the north, hot anomalies of the Khangai plume and the Khentei Plateau break through to the surface. Around these anomalies, some cold fragments of positive δV_p anomalies can be observed (Fig. 7, north of 40° N).

Another sublongitudinal section across Hindustan and Central Asia shows that the cold body of the Indian Platform is dipping beneath the Himalayas and southern Tibet as deep as 700 km (Fig. 8).

The cold upper mantle (50–200 km) lens between Tibet and the Khangai plume and north of it is traced beneath the Siberian Platform (55° N) to depth of at least 400 km.

"Hot" bodies:

— the Tibet plume, a funnel up to 750 km with insignificantly lower δV_p values to a depth of 1100 km and even more lowered values up to 1700 km;

— the Khangai plume, from Gobi Altai; the roots are located in the south at depths up to 800 km and less pronounced at depths up to 1200 km; the deep connection of the plume to a branch of the Pacific superplume is assumed.

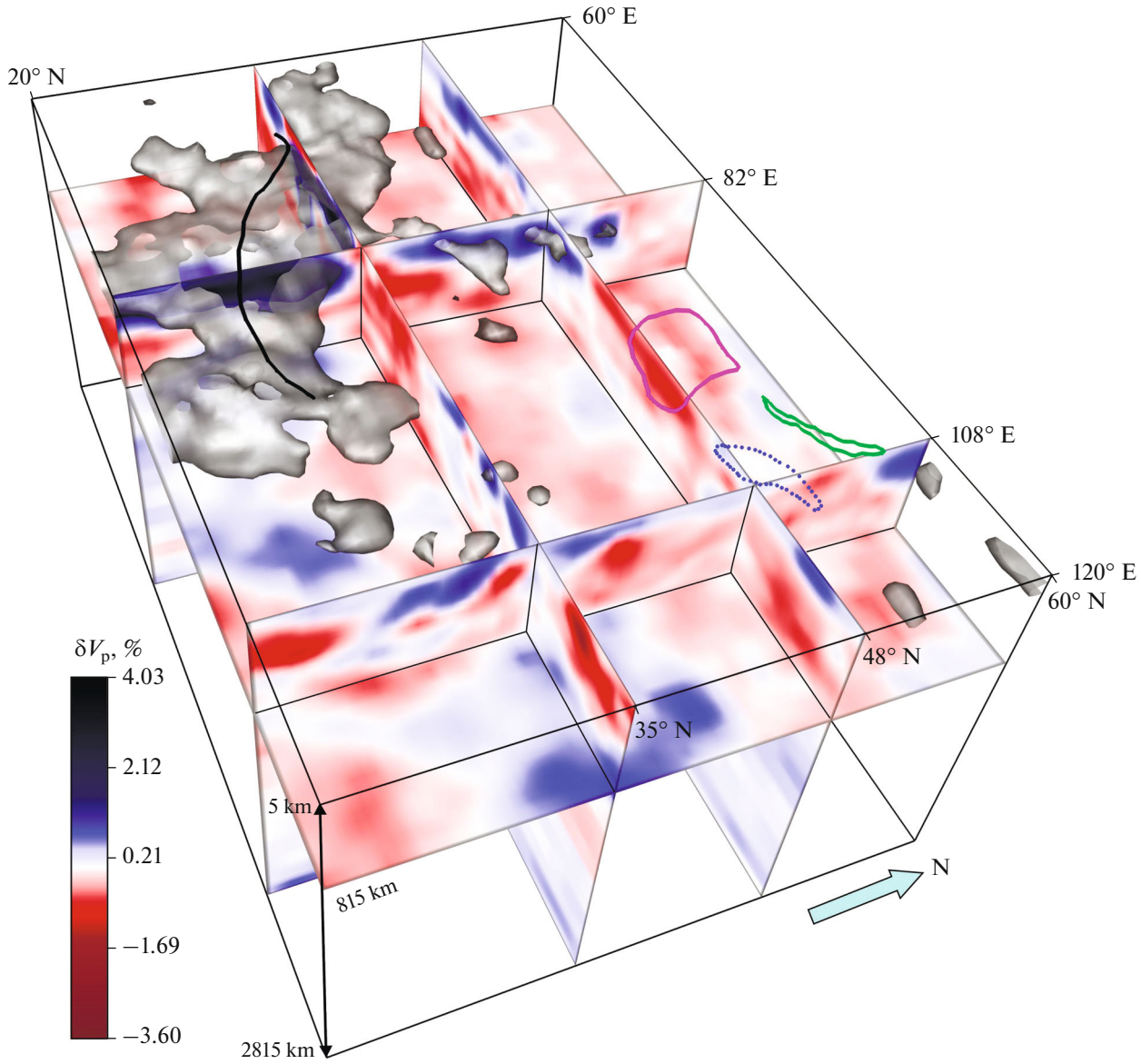

Fig. 7. 3D visualization of δV_p velocity variations in Central Asia based on UU-P07 model data [17, 26, 36]. Viewpoint is located in southeast and is oriented to depth from surface; isosurface is shown for positive variation values of 1.26% with partial transparency. Lake Baikal is outlined in green; Khangai Plateau, in purple; Khentei Plateau, in blue; southern flank of Himalayas, in black.

Structure of Mantle Heterogeneities in the Study Area

The vast area of stagnant slabs in the inner part of the Sunda arc is bounded by the intrusion of sublatitudinal hot bodies of the South China and, to a lesser extent, Andaman seas, along which modern rift segments develop on the surface (Figs. 1, 4).

According to the viewpoint expressed in [32], a toroidal mantle flow rises to the area through a gap in the flat slab. The latter formed a sublatitudinal weak area ~40 Ma ago, in which mantle upwelling was focused and the rift-related area became expanded. This view is supported by the ages of paleorift segments located to the east (~42 Ma) and west (~32 Ma) of the back-arc area (Fig. 1).

However, the formation of this back-area area should be accompanied by lateral displacement of mantle upwelling zone toward the latter and a complete termination of sublatitudinal rifting beyond it. It seems that another mechanism capable of forming a gap in a flat slab and of launching secondary (upper mantle) plumes is rollback one [6]. Simultaneous action of both mechanisms is also not excluded.

The sublatitudinal mantle section shows the flat-topped stagnant slabs and its layered structure in a depth interval from ~700 to ~1500 km (Fig. 5). The space above the top of the slab includes local hot mantle bodies, which are considered secondary plumes. The latter form local rift segments [20] and are often recorded above the stagnant slabs (Fig. 1).

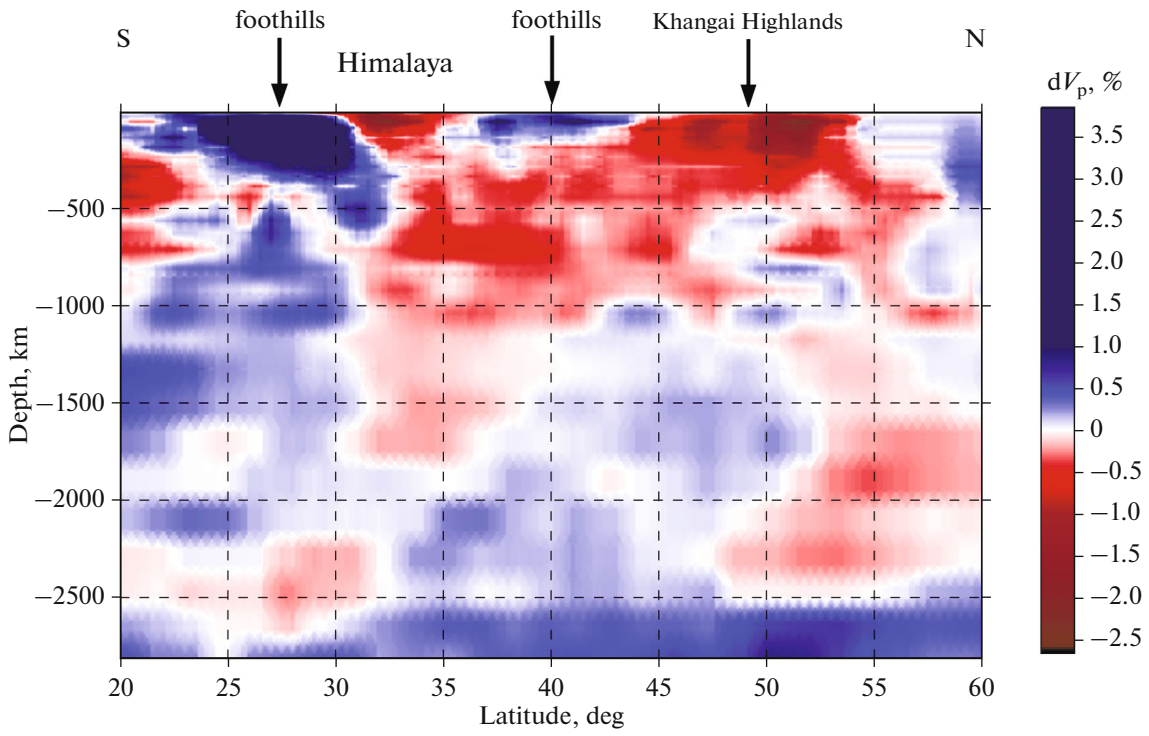

Fig. 8. Seismotomographic section along sublongitudinal profile according to UU-P07 model [17, 26, 36]. For position of profile, see Fig. 9.

A weak negative variation in δV_p was recorded in the eastern part of the section near the branch of the Pacific superplume. In the western part of the section beneath the Ninetyeast Ridge and further west, a rather rare configuration of a hot mantle body was recorded in a depth interval from 500 to 1000 km. This body is confined to the Indian Ocean Geoid Low and the known zone of intraplate deformation [28].

The uplift of this minimum is disrupted by a slab of the western part of the Sunda arc. Nevertheless, according to the hypothesis of the influence of a "mantle wind" affecting this slab through a window in the slab, its probable association with hot body in the back-arc basin remains observable [32].

The sublongitudinal section also emphasizes the layering of the slab in the space to the east of the Sunda Trench (Fig. 6). In addition, the section illustrates the break in a slab and hot mantle plumes, which break through to the surface. This breakthrough zone has a complex configuration. It shows signs of upwelling of hot masses from a depth of ~2000 km, which are considered to be the western branch of the Pacific superplume.

In a depth interval from 1000 to 500 km, one can observe a strengthening of negative δV_p anomalies and their lateral localization that lead to the formation of upper mantle secondary plumes [20]. It is unclear whether the small cold δV_p anomalies in this area are random variations or we deal with fragments of a ruptured subhorizontal slab. A similar pattern is observed to the north of 40° N near the Khentei Plateau. A possible relationship with the Pacific superplume and a horizontal bridge with the Tibet plume are also observable in this area.

Analysis of the structure of the upper mantle, transition layer, and the upper part of the lower mantle of the entire study area allows us to distinguish structurally ordered bodies with reduced and increased δV_p velocities.

Two types are distinguished among bodies with reduced velocities (hot bodies):

— bark-arc anomalies;

— intramantle plumes.

Back-arc hot bodies do not extend deeper than the upper mantle and its transition layer, having a discontinuous distribution in the transition layer. Intramantle plumes—Tibet and Khangai—are well defined at depth as deep as 750–800 km, but their root part with less reduced seismic wave velocities reach depths of 1100–1700 km. No single clearly pronounced root is observed in these plumes. Probably, they have several weakly pronounced roots.

The structures of the subduction zones in front of the Himalayas and the Sunda arc are similar in that in both cases the cold upper mantle mass of the subducting plate submerge into a cold subducting slab, which is traced to depths of 700 km (the Himalayas) and 850 km (the Sunda arc). However, these regions differ significantly in the structure of their prefrontal parts.

Ahead of the Himalayan front, the thickness of the cold upper mantle part of the Indian Platform, which begins immediately below the crustal basement, increases from 150 to 300 km as it approaches the slab.

In front of the Sunda arc, the thickness of the cold upper mantle part of the subducting Indian Plate does not increase, being ~100 km. In front of the subduction zone, it is underlain by a body with a sharply decreased δV_p, which is dipping southwestward beneath the Ninety East Ridge to a depth of 750–850 km. The northern part of the Sunda subduction zone cuts the intramantle plume upwelling from a depth of ~1150 km (Fig. 6). Its deepest part (inferred root) is located to the north of the intersection of sections near the Malacca Peninsula (Figs. 4, 5).

This plume (let us call it the Indosinian plume) connects in the north with the eastern part of the Tibet plume and continues to the south as a part of the sublongitudinal series, represented by the Tibet and Khangai plumes.

ROCK MASS MOTION VECTORS IN EARTHQUAKE SOURCES OF THE SUNDA AND HIMALAYAN ARCS

Sunda Arc

The Sunda arc is traditionally interpreted as a subduction zone of the Indian Ocean lithosphere (as a part of the Indian Plate) beneath the southeastern margin of Asia and adjacent back-arc basins. According to the models available, the plate is subducting in the northeastern direction (~35°), perpendicular to the central part of the arc. In such a case, only subduction should be observed in this part of the arc, while in the marginal parts of the arc, oriented obliquely to the direction of plate motion, subduction should be combined with or replaced by shear displacement.

To check the validity of this model, we used the azimuths of rock mass displacements along the fault planes in earthquake sources that occurred in the Sunda arc area during the last half a century. The method applied does not allow one to distinguish the subduction from the thrust, but indicates the displacement azimuth (Table 1, Fig. 2).

A comparative analysis of the azimuths of the identified earthquake-induced displacements revealed their significant differences from the above model (Table 1).

In arc segment 1, as follows from the model and is consistent with the presence of the active Sagaing dextral strike-slip fault extending along the arc, dextral displacements with a subduction component dominate (Table 1, arc segment 1).

However, in addition to these, there are thrusts or underthrusts with a shear component, which are equally significant. The dip azimuths of the latter range from 210° to 250°; i.e., they are partially different from the dip azimuth of the model underthrust plane of 215°.

In segment 2, this deviation of the arc becomes more prominent (Table 1, arc segment 2).

Here, a strike-slip fault with underthrust, corresponding to the above model, is present. However, thrusts with a dip azimuth of 260°, which is close to the normal strike of the segment 280°–285°, become a critical component. However, this dip azimuth is significantly different from the model one of 215°.

Segment 3 is also characterized by a dextral strike-slip component, sometimes with a subduction component, consistent with the model one (Table 1, arc segment 3).

As well, thrusts or underthrusts with displacement azimuths of 200°–250° dominate. They can be interpreted partly as underthrusts with an azimuth of 215° close to the model one and partly as thrusts in a direction close to 255°, at the normal to the arc strike.

Segment 4, where the 45°–50° normal vector to the arc strike is close to the direction of model underthrusting, is dominated by thrust faults or underthrust ones with displacement azimuths of 200°–280° (Table 1, arc segment 4).

This can be equally interpreted as the Indian Plate underthrust and counterthrust of the Sunda arc corresponding to the model. At this, a higher degree of seismicity can be explained by the combined effect of both factors.

Segment 5 is sharply dominated by numerous thrust-induced seismic events with movement azimuths of 190°–200° (Table 1, arc segment 5).

These azimuths are noticeably different from the model thrust direction and close to normal to the 190° strike.

The same situation is observed in segment 6, in which thrust-induced earthquakes with movement azimuths of 170°–180° dominate with a normal strike of the segment of 180°. This is significantly different from the model azimuth of underthrusting (Table 1, arc segment 6).

In segment 7, which is dominated by thrust faults with displacement azimuths of 170° ± 10° at 170°–175° normal to the segment strike, this difference is even greater (Table 1, arc segment 7).

The situation changes in segment 8, which is WSW–ENE-trending (Table 1, arc segment 8).

This segment is dominated by thrust faults with displacement azimuths of 170° ± 10° at the normal to the segment strike of 160°–165°. Simultaneously, a significant role is played by sinistral thrusts with a underthrust component; the displacement azimuths of 50° ± 20°.

In all segments of the Sunda arc, except for segment 1, reverse (antithetical) thrust-induced earthquakes are present in a subordinate number. Their displacement azimuths in each segment differ from the predominant azimuths by about 180° (Table 1).

Table 1. Directions of seismic movements in Sunda arc

Ser. No.	Segment of arc	Strike, °	Perpendicular to strike of segment, °	Predominant directions of displacements, °	Displacement kinematics
	1	*2*	*3**	*4***	*5***
1	25°–18° N	0–10 = 180–190	90–100 = 270–280	340–350 (210–250)	Dextral strike slip and thrust fault (strike slip and thrust fault)
2	15°–10° N	10–15 = 190–195	100–105 = 280–285	260–160 (70–100)	Thrust and dextral strike-slip fault (strike-slip fault and thrust – reverse thrust with strike-slip fault)
3	10°–5° N	345 = 165	75 = 255	200–250 (150–160); 350–300 (70–100)	Thrust (strike slip and thrust fault); Dextral strike-slip fault (reverse thrust)
4	5° N–6° S	315–320 = 135–140	45–50 = 225–230	200–280 (30–70)	Thrust fault (reverse thrust)
5	105°–115° E	280 = 100	10 = 190	190–200 (10–20)	Thrust fault (reverse thrust)
6	115°–120° E	270 = 90	0 = 180	170–180 (350–10)	Thrust fault (reverse thrust)
7	120°–125° E	80–85 = 260–265	350–355 = 170–175	170 ± 10 (340–350)	Thrust fault (reverse thrust)
8	125°–133° E	70–75	340–345 = 160–165	170 ± 10; 50 ± 20 (340–20)	Thrust fault; sinistral strike-slip fault with underthrust fault (reversed thrust)

* First equality values indicate potential direction of subduction beneath arc; second equality values indicate potential direction of thrusting onto slab; ** displacements (thrusts) leading to uplift of hanging wall independently of thrusting or subduction along fault planes; rare orientation of displacement azimuths is given in brackets.

Thus, in all segments of the arc are traces of seismic movements (seismic flow, according to [11]), consistent with the model of the Indian Plate subduction beneath the arc. They are represented by a thrust–underthrust combination, which can be interpreted as plate subduction northeastward (35° ± 10°), with dextral strike-slip faults in longitudinal northern segments 1 and 2 and sinistral strike-slip faults in eastern segment 8 extending east-northeastward (Table 1).

Along with these movements, however, there are traces of thrust-underthrust tectonics in the direction frontal to the strike of each arc segment. Taking into account its curvature, these movements can be interpreted as the result of the arc thrusting on the Indian Plate.

In segments 2 and 5–8, the number of thrust-induced seismic events exceeds that of events induced by the Indian Plate subduction (Table 1).

In segments 3 and 4, where the arc extends approximately normal to the direction of subduction, it is impossible to distinguish it from manifestations of reverse thrusting using the given method used (Table 1).

However, a significant increase in the total number of earthquakes with thrust-underthrust mechanisms indicates a combination of these sources of seismic events. Arc thrusting is accompanied by less numerous antithetic thrust movements. They form a belt, which is approximately parallel to the thrust belt being different from it by 180°.

The seismic data obtained indicate that along with the subduction of the Indian Plate beneath the Sunda arc, transverse shortening of this arc and its widespread thrusting onto the Indian Plate are recorded.

Himalayan Arc

The Himalayas form a south westwardly convex arc (Fig. 9).

According to model constructions, based on GPS measurements, in addition to the postulates of plate

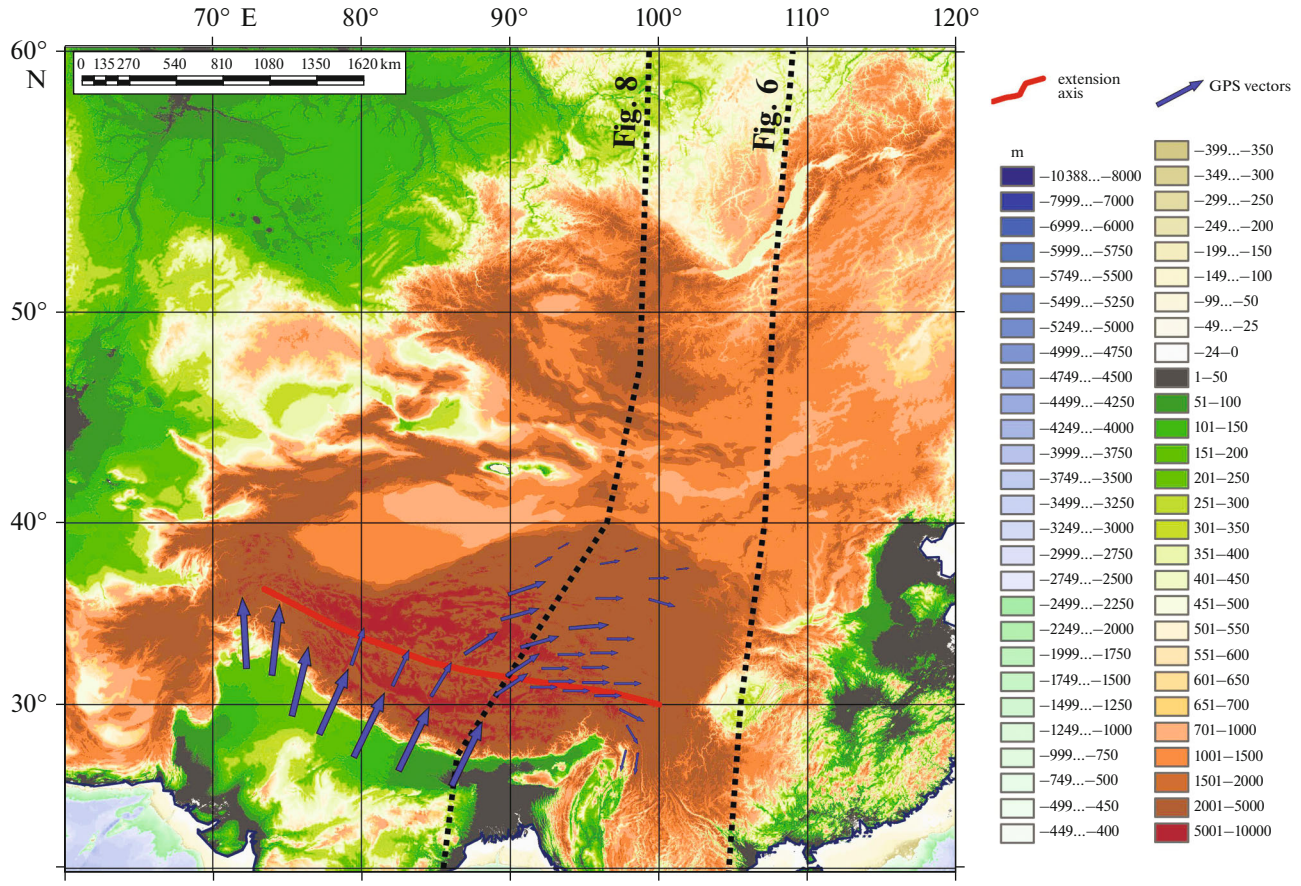

Fig. 9. Scheme of horizontal motion of lithospheric plates and blocks in Hindustan–Tibet collision zone, compiled from GPS data (after [22, 27, 39]). For position of sections (dashed line) see Figs. 6 and 8; axis of horizontal extension and strike-slip fault is marked by red line (after [2, 10, 37]).

tectonics, the Indian Plate is subducting beneath the Himalayas. In the central, most extended part of the arc, the direction of northeastern thrusting is 25°.

The direction becomes sublongitudinal (350°) on the northwestern flank of the arc, near the Punjab Syntaxis.

On the eastern flank of the arc, there occur more complex changes due to the north-northeastward movement of the Assam wedge of the Indian Platform.

There are much fewer earthquakes in the Himalayas than in the Sunda arc. Due to this, the distribution pattern of seismic movements is vaguer and discontinuous. Nevertheless, some trends are recorded (Fig. 10).

The largest number of earthquakes is recorded in the northwest of the arc and in the Punjab Syntaxis. Here, between 70° and 72° E, most seismic movements occur in the 200°–250° (20°–70°) direction and correspond to thrust–underthrust fault perpendicular to the arc front.

In the 50°–70° direction, the displacements obtain a dextral strike-slip component associated with Karakorum dextral shear movements. Along with this, there are thrust–underthrust movements in the direction of 330°–350°, corresponding to the model constructions.

Between 68° and 70° E, conjugate displacements in the 100° and 280°–300° directions are also present, reflecting movements on the western flank of the Syntaxis.

At the 80°–88° E segment, the arc is dominated by displacements in the 200° (20°) direction, which can be interpreted equally as the subduction of the Indian platform and thrust tectonics of the Himalayas.

Between 90° and 96° E, at the northwestern flank of Assam, two directions of displacement are distinguished (Table 1):

— 210°–240° (30°–60°) direction corresponding to longitudinal sinistral strike-slip fault;

— 120°–140° (300°–320°) direction corresponding to thrust-underthrust normal to the Assam front.

Between 97° and 100° E, northward of the eastern flank of the Assam wedge, two directions of displacement are distinguished:

— 200° (20°) direction, which can be interpreted as thrust-underthrust, normal to the front of the Assam wedge;

— ~350° (170°) direction, which can be interpreted as dextral strike-slip fault.

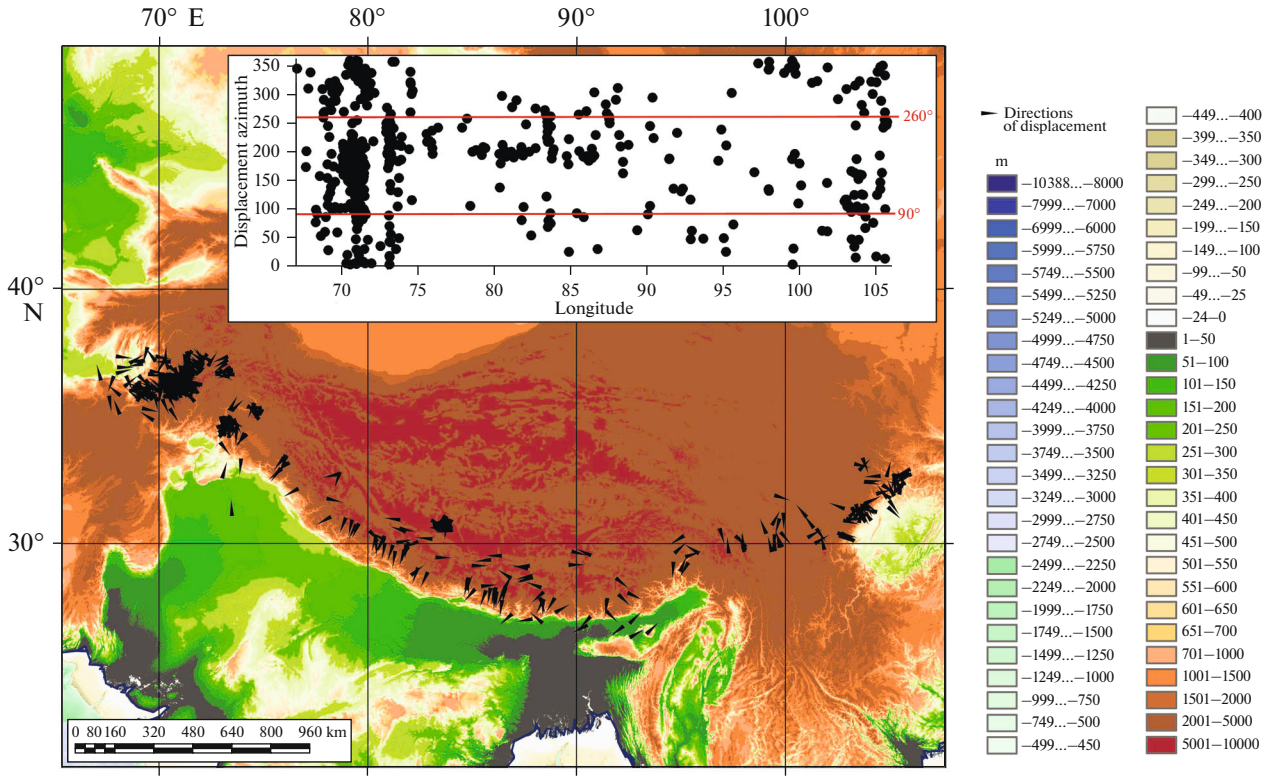

Fig. 10. Azimuths of displacements along strong earthquake fault planes according to CMT catalog [24, 39]. Inset: swarm of displacement azimuth points along Himalayan front.

Thus, two directions of seismic movements are distinguished in the Himalayan arc. The first direction corresponds to the Indian platform subduction model, complicated by the reorientation of seismic flow at the Punjab and Assam flanks of the arc. The second direction combines displacements normal to the Himalayan front, and we believe that the second direction, as in the Sunda arc reflects the thrust of the Himalayas onto the Indian Platform.

RESULTS

Neotectonic Kinematics of the Sunda and Himalayan Arcs

According to plate tectonics theory, the displacement vector along the convergent plate boundary should be tangent to small circles on the surface of a rotating spheroid with respect to their Euler pole [25].

The real distribution of the displacement azimuths along the fault planes of the Sunda arc region does not correspond to this position (Fig. 2). They are directed outward from the center of the arc curvature. In our opinion, this indicates the presence of thrust processes at the arc front, not related to the subducting plate, which significantly complicate the modern geodynamics.

Therefore, let us mention the observation of A.N. Mazarovich [7] concerning the interaction of lithospheric plates in the Northwest Pacific Ocean, where the edge of the continental lithosphere is thrust over the ocean floor. At this, the arcuate shape of island chains represents the projection of rectilinear thrust planes on the geoid surface, which certainly has the arcuate shape. Thus, the genesis of the arcs is determined by the thrusting of the continental lithosphere onto the oceanic lithosphere.

The orientation of the movements along the Sunda Trench changes in a fan-shape arrangement from its northwestern edge to the southeastern one (Fig. 2). In each segment of the trench, a statistically significant number of measured directions have an orientation orthogonal to the trench itself. The distribution of azimuths along the trench strike shows a regular change from the transition zone, from the Sagaing strike-slip fault to the southeastern edge of the trench, from 260° to 160°, respectively (Fig. 2, inset).

The ~100° reversal is observed. The azimuths are directed toward the oceanic part. In addition, the main swarm of azimuths is duplicated with a difference of 180°. This shows that along with the main thrust displacements, a parallel group of antithetic thrust events occurs (Fig. 2, inset). A chain with an azimuth difference of ~90° is traced between the main swarm and the duplicated one with a significantly

smaller number of seismic events. This chain most likely reflects the shear slip [25] that arises from the non-orthogonal orientation of the oceanic plate motion vector toward the trench. This is indicated by the complete attenuation of this chain in the ~105° area, where the displacement azimuth of the Indo-Australian plate is orthogonal to the trench, and its appearance further eastward (Fig. 1).

Note also that the dominant thrusting, normal to the front of the Sunda arc, is directed toward the subducting plate. This process is combined with an abundance of hot and, consequently, low density mantle masses associated with both the intramantle Indo-Australian plume and the plume-type upper mantle formations, characteristic of the Andaman back-arc sea, and controlling the development of rift-related structures in the latter. The extension of the back-arc basin could have caused the thrusting of the Sunda arc. The Himalayan arc is the modern collisional boundary between Hindustan and the Eurasian Plate. The GPS vector field in the arc region has a fan-shaped reversal from ~355° in the west of the arc to ~30° in the east with a general northern displacement azimuth of the near-surface blocks [22, 27] (Figs. 7, 9).

The orientation of the displacement directions in the Himalayan arc changes in the shape of a fan from its northwestern edge to the southeastern one (Fig. 9).

Despite the smaller number of seismic events, the same pattern of change in the displacement azimuths along the strike of the Himalayan and Sunda arcs is observed (Figs. 2, 10).

At each segment of the trench, azimuths are oriented orthogonal to the latter. The distribution of azimuths along the trench strike shows their regular change from 70° to 105° N (Fig. 10, inset).

A ~170° reversal occurs (from 260° to 90°). The azimuths of thrusting are directed toward Hindustan. In addition, the main swarm of azimuths is duplicated with a 180° difference, as well as along the Sunda arc, showing the presence of a small number of antithetic thrust fauly-induced events (Fig. 10, inset).

In the back-arc area, north of the Himalayan arc, are the Tibet intramantle plume and the Tibet extensional plateau [2, 10, 13, 37]. It is possible that here, as in the Sunda arc, modern thrust process is associated with back-arc extension.

DISCUSSION

An Indosinian intramantle plume rising from a depth of ~1150 km is identified in Southeast Asia east of the northern part of the Sunda arc. It continues southward as a part of the N-S-trending series of similar plume formations represented northward by the Tibet and Khangai intramantle plumes.

At the same time, a vast high-velocity mantle area at depths from ~700 to ~1500 km is distinguished between the Sunda and Mariana island arcs. This area can be regarded as a combination of stagnant segments of subducting slabs in separate subduction zones of the region. Mantle sections show the flat top of the united stagnant slab and its layered structure. The stagnant slab area is interrupted by the intrusion of W-E-trending hot volumes of South China and, to a lesser extent, the Andaman Sea.

One of the possible mechanisms resulting in such a mantle structure is toroidal mantle flow through a gap in the flat-topped slab. Another mechanism capable of forming a gap in a flat slab and lunching secondary (upper mantle) plumes is rollback. Both mechanisms can manifest simultaneously. The space above the top of the slab comprises local hot mantle bodies, which are considered secondary plumes. They are often recorded above the stagnant slabs and contain local rift segments.

The visualization of δV_p velocity variations within Tibet and Central Asia contains structural patterns similar to the reference area of the Sunda arc. A vast area of subhorizontal fragments of laterally different slabs and a gap, which is characterized by plume anomalies of deep and secondary origin, is observed. The branches of the Khangai plume, which have no roots deeper than 1000 km, but connected with the Tibet plume by horizontal bridges, are traced to the north to Lake Baikal.

A weak negative variation in δV_p is detected between the Sunda and Mariana island arcs, possibly reflecting a branch of the Pacific superplume. A similar pattern is observed north of 40° N near the Khentei Plateau. In this area, a possible link between the Khangai intramantle plume and the Pacific superplume and the Tibetan intramantle plume was identified.

Vectors of rock mass movement along the majority of fault planes during earthquakes in the Sunda arc are directed outward from the center of arc curvature. This indicates that along with the subduction of the Indian Plate beneath the Sunda arc, there is a transverse shortening of the latter and its widespread thrusting onto the Indian Plate is not connected with the underthrusting plate. The arc thrusting is accompanied by rare displacements along antithetic thrust faults. As evidenced from displacement azimuths, they form a belt, which is approximately parallel to the thrust belt, being different from the latter by 180° (Fig. 2, inset).

There are two groups of seismic movements in the Himalayan arc:

— The first-group displacement azimuths, together with the GPS vectors, are directed towards the Tibet plume and correspond to the Indian platform underthrusting model. This group has a fan-shaped distribution due to the reorientation of underthrusting on the Punjab and Assam flanks of the arc.

— The second group of displacement azimuths combines displacements normal to the Himalayan front. As in the Sunda arc, the second group probably

reflects the thrusting of the Himalayas onto the Indian Platform.

A N-S-trending section through Hindustan and Central Asia shows that Central Tibet contains an intramantle plume, extending toward the surface, and an extension zone above it. A similar configuration is observed in the reference region of the Sunda arc. The bark-arc zone is dominated by upper mantle bodies with reduced *P*-wave velocities, accompanied by the formation of the Andaman Sea rifts. This comparison provides an assessment of the role of thrusting processes in subduction zones that complement the multifactor interaction in a geodynamically active environment.

As a result of this study, we suggest that the back-arc negative δV_p variation reflects the subsurface extension of the upper mantle hot body with the formation of thrusts of the Sunda and Himalayan arcs and extension zones in back-arc zones. Local rift segments, sometimes transforming into spreading systems, are formed in the areas where such plumes are manifested.

CONCLUSIONS

(1) In Southeast Asia, east of the northern part of the Sunda arc, the Indosinian intramantle plume rising from a depth of ~1150 km has been identified. It continues southward as part of the N-S-trending series of similar plumes, represented northward by the Tibet and Khangai intramantle plumes.

At the same time, a vast area of the stagnant slabs in the inner part of the Sunda arc is interrupted by the intrusion of W-E-trending hot bodies of the South China Sea and, to a lesser extent, the Andaman Sea. One of possible mechanisms for this mantle structure is toroidal mantle flow through a gap in a flat slab. It seems that another mechanism capable of forming a gap in a flat slab and of launching secondary (upper mantle) plumes is rollback one. Simultaneous action of both mechanisms is also not excluded.

(2) The mantle sections show the flat top of the stagnant slabs and their layered structure in the depth interval from ~700 to ~1500 km. The space above the top of the slab includes local hot mantle bodies, which are considered secondary plumes. They are often recorded above stagnant slabs and form local rift segments.

A weak negative variation of δV_p is also observed near the branch of the Pacific superplume. A similar pattern is observed north of 40° N near the Khentei Highlands. This region also has a possible connection with the Pacific superplume and a horizontal link with the Tibet plume.

(3) The visualization of δV_p velocity variations in the Tibet and Central Asian areas shows structural patterns similar to the reference region of the Sunda arc. A vast area of subhorizontal fragments of laterally different slabs and a gap are observed, which is characterized by plume anomalies of deep and secondary origin. The branches of the Khangai plume, which have no roots deeper than 1000 km, but are connected with the Tibet plume by horizontal links, are traced north to Lake Baikal. A vast area of subhorizontal slab fragments of varying lateral size and discontinuity is observed, where plume anomalies of deep and secondary origin have been established.

(4) The vectors of rock mass movements along the fault planes of the Sunda arc are directed outward from the center of arc curvature. This indicates the development of thrust processes at the arc front, not related to the subducting plate. The displacement azimuths, in addition to the main field of values, are duplicated with a difference of 180°. This is associated with antithetic thrusts, which are also orthogonal to the orientation of the trench in each of its segments.

(5) The given seismological data indicate that, along with the subduction of the Indian Plate beneath the Sunda arc, transverse shortening of the arc and its widespread thrusting onto the Indian Plate have been recorded.

(6) The fan-shaped reversal of the displacement azimuths along the Himalayas is directed toward Hindustan. The fan-shaped reversal of GPS vectors along the Himalayas is directed toward Tibet. This shows that the main indicator of tectonic activity (seismic events) has a direction of rock mass displacement to the south from the extensional back-arc basin within Tibet with the development of thrust deformation during movements along the detachment planes.

(7) Two directions of seismic movements are distinguished in the Himalayan arc. The first direction corresponds to the Indian Platform subduction model, being complicated by the reorientation of seismic flow on the Punjab and Assam flanks of the arc. The second direction integrates movements normal to the Himalayan front, which, as in the Sunda arc, reflects the thrusting of the Himalayas onto the Indian Platform.

(8) A N-S-trending section through Hindustan and Central Asia shows that central Tibet contains a plume in the extension zone extending toward the surface. Since the same configuration of the plume in the slab rupture region is also seen in the reference region of the Sunda arc, it is possible to suggest that this mantle anomaly leads to the expansion of the hot body near the surface with the formation of thrusts along the arcs and extension zones in their back-arc zone. Local rift segments, sometimes transforming into spreading systems, are formed in areas where such plumes are manifested.

ACKNOWLEDGEMENTS

Authors are thankful to reviewer A.I. Kozhurin (Institute of Volcanology and Seismology, Far East Branch RAS, Pet-

ropavlovsk-Kamchatsky, Russia) and anonymous reviewer for helpful comments, authors extend their gratitude to editor M.N. Shoupletsova (Geological Institute RAS, Moscow, Russia) for thorough editing.

FUNDING

This study was supported by the Russian Science Foundation (project no. 22-17-00049 "Neotectonics and Active Tectonics in Northern Central Asia").

CONFLICT OF INTEREST

The authors of this work declare that they have no conflicts of interest.

REFERENCES

1. K. Aki and P. Richards, *Quantitative Seismology: Theory and Methods* (MIR, Moscow, 1983).
2. R. S. Alekseev and Yu. L Rebetsky, "Model of the evolution of the lithosphere of the Himalayan–Tibet Orogen," *Vestn. KRAUNTs. Nauki Zemle* **52** (4), 89–107 (2021).
3. A. A. Belov, Yu. G. Gatinskii, and A. A. Mossakovskii, "Indosinides of Eurasia," Geotektonika, No. 6, 21–42 (1985).
4. V. S. Burtman, Tectonics and geodynamics of Tian Shan and the High Asia in the Paleozoic, in *Transactions of Geological Institute of Russian Academy of Sciences*. Vol. 570, Ed. by A. A. Mossakovsky (GEOS, Moscow, 2006) [in Russian].
5. D. Zhao, F. Pirajno, and L. Liu, "Mantle structure and dynamics under East Russia and adjacent regions," Russ. Geol. Geophys. **51** (9), 925–938 (2010).
6. L. I. Lobkovskii, M. V. Kononov, and E. V. Shipilov, "Geodynamic causes of the emergence and termination of Cenozoic shear deformations in the Khatanga–Lomonosov Fault Zone (Arctic)," Dokl. Earth Sci. **492**, 356–360 (2020).
7. A. N. Mazarovich, *Foundations of Geology of the USSR* (ONTI NKTP SSSR, Moscow–Leningrad, 1938).
8. A. A. Mossakovsky, S. V. Ruzhentsev, S. G. Samygin, and T. N. Kheraskova, "The Central Asian Orogenic Belt: Geodynamic evolution and history of formation," Geotektonika, No. 6, 3–32 (1993).
9. L. M. Parfenov, N. A. Bepzin, A. I. Khanchuk, G. Badarch, V. G. Belichenko, A. N. Bulatov, S. I. Dril, G. L. Kirillova, M. I. Kuzmin, W. Nokleberg, A. D. Prokopiev, V. F. Timofeev, O. Tomurtogoo, and X. Yan, "Model of orogenic belt formation in Central and Northeast Asia," Tikhookean. Geol. **22** (6), 7–41 (2003).
10. Yu. L. Rebetsky and R. S. Alekseev, "The field of recent tectonic stresses in Central and Southeastern Asia," Geodynam. Tectonophys. **5** (1), 257–290 (2014). https://doi.org/10.5800/GT-2014-5-1-0127
11. Yu. V. Riznichenko, "Calculation of strain rates for seismic flow of mountain masses," Izv. Akad. Nauk SSSR. Fizika Zemli, No. 10, 34–47 (1977).
12. S. Yu. Sokolov and V. G. Trifonov, "Role of the asthenosphere in transfer and deformation of the lithosphere: The Ethiopian-Afar superplume and the Alpine–Himalayan Belt," Geotectonics **46** (3), 171–184 (2012).
13. V. G. Trifonov, E. A. Zelenin, S. Yu. Sokolov, and D. M. Bachmanov, "Active tectonics of Central Asia," Geotectonics **55** (3), 361–376 (2021).
14. V. G. Trifonov, S. Yu. Sokolov, D. M. Bachmanov, S. A. Sokolov, and Ya. I. Trikhunkov, "Neotectonics and the upper mantle structure of Central Asia," Geotectonics **55** (3), 334–360 (2021).
15. V. E. Khain, *Tectonics of Continents and Oceans* (Nauchn. Mir, Moscow, 2001).
16. J. C. Aitchison, J. R. Ali, and A. V. Davis, "When and where did India and Asia collide?" J. Geophys. Res. **112** (B05423), 1–19 (2007).
17. M. Amaru, *Global Travel Time Tomography with 3D Reference Models. PhD Thesis* (Geol. Departm., Utrecht Univ., Germany, 2007) (in German).
18. D. F. Argus, R. G. Gordon, and C. DeMets, "Geologically current motion of 56 plates relative to the no-net-rotation reference frame," Geochem., Geophys., Geosyst. **12** (11), 1–13 (2011).
19. T. W. Becker and L. Boschi, "A comparison of tomographic and geodynamic mantle models," Geochem., Geophys., Geosyst. **3**, 1–48 (2002). https://doi.org/10.129/2001GC000168
20. S. Cloetingh, A. Koptev, A. Lavecchia, I. J. Kovacs, and F. Beekman, "Fingerprinting secondary mantle plumes," Earth Planet. Sci. Lett. **597**, Art. **117819**, 1–16 (2022).
21. M. Gaetani, "The Karakorum Block in Central Asia, from Ordovician to Cretaceous," Sediment. Geol. **109**, 339–359 (1997).
22. W. Gan, P. Molnar, P. Zhang, G. Xiao, S. Liang, K. Zhang, Z. Li, K. Xu, and L. Zhang, "Initiation of clockwise rotation and eastward transport of Southeastern Tibet inferred from deflected fault traces and GPS observations," GSA Bull. **134** (5–6), 1129–1142 (2021). https://doi.org/10.1130/B36069.1
23. S. E. Graham, J. P. Loveless, and B. J. Meade, "Global plate motions and earthquake cycle effects," Geochem., Geophys., Geosyst. **19**, 2032–2048 (2017).
24. Global CMT Catalog. 2018. www.globalcmt.org/CMTsearch.html (Accessed October 31, 2018).
25. M. Guzman-Speziale, "Oblique plate convergence along arcuate trenches on a spherical Earth. An example from the Western Sunda Arc," Acta Geophys., 1–21 (2023). https://doi.org/10.1007/s11600-023-01163-9
26. R. Hall and W. Spakman, "Mantle structure and tectonic history of SE Asia," Tectonophysics **658**, 14–45 (2015).
27. M. Hao, Y. Li, and W. Zhuang, "Crustal movement and strain distribution in East Asia revealed by GPS observations," Nat. Sci. Rep. **9**, Art. 16797 (2019). https://doi.org/10.1038/s41598-019-53306-y
28. *Intraplate Deformation in the Central Indian Ocean Basin*, Ed. by Yu. P. Neprochnov, G. D. Rao, C. Subramaniyam, and K. S. R. Murthy (Geol. Soc. India, 1998, Vol. M-39).
29. H. Kárason and R. D. Van Der Hilst, "Constraints on mantle convection from seismic tomography, in *The*

History and Dynamics of Global Plate Motions, Ed. by M. A. Richards, R. G. Gordon, and R. D. Van Der Hilst (AGU, Geophys. Monogr. Ser., 2000, Vol. 121), pp. 277–288. https://doi.org/10.1029/GM121p0277

30. M. P. Searle, *Geology and Tectonics of the Karakorum Mountains*, Ed. by B. F. Windley (Wiley, Chichester, UK, 1991).
31. W. J. Su and A. M. Dziewonski, "Simultaneous inversion for 3D variations in shear and bulk velocity in the mantle," Phys. Earth Planet. Interior **100** (1–4), 135–156 (1997).
32. Y. Suo, H. Dong, L. Liu, D. Peng, Y. Li, J. Liu, L. Dai, X. Cao, and S. Li, "Landward mantle flow associated with the Pacific subduction system opened the South China Sea," Res. Square (2022). https://doi.org/10.21203/rs.3.rs-2332418/v1
33. S. Susilo, I. Meilano, H. Z. Abidin, B. Sapiie, J. Efendi, and A. B. Wijanarto, "Velocity Field from Twenty-Two Years of Combined GPS Daily Coordinate Time Series Analysis," AIP Conf. Proc., Art. 1730.040003, 1–4 (2016).
34. A. Todrani, F. Speranza, N. D'Agostino, and B. Zhang, "Post-50 Ma Evolution of India–Asia collision zone from paleomagnetic and GPS data: Greater India indentation to eastward Tibet low," Geophys. Rev. Lett. **49**, 1–16 (2021). https://doi.org/10.1029/2021GL096623
35. G. Toyokuni, D. Zhao, and K. Kurata, "Whole-mantle tomography of Southeast Asia: New insight into plumes and slabs," J. Geophys. Res.: Solid Earth **127** (11), 1–29 (2022). P. 1–29. https://doi.org/10.1029/2022JB024298
36. D. G. Van der Meer, D. J. Van Hinsbergen, and W. Spakman, "Atlas of the underworld: Slab remnants in the mantle, their sinking history, and a new outlook on lower mantle viscosity," Tectonophysics **723**, 309–448 (2018).
37. L. Wang and S. Barbot, "Three-dimensional kinematics of the India–Eurasia collision," Nat. Commun.: Earth Environ. **164** (4), 1–13 (2023). https://doi.org/10.1038/s43247-023-00815-4
38. M. Wang and Z. K. Shen, "Present-day crustal deformation of continental China derived from GPS and its tectonic implications," J. Geophys. Res.: Solid Earth **125** (2), 1–22 (2020). https://doi.org/10.1029/2019JB018774
39. GEBCO 30" Bathymetry Grid. Version 20141103. 2014. http://www.gebco.net) (Accessed February 23, 2022).

Translated by D. Voroshchuk

Publisher's Note. Pleiades Publishing remains neutral with regard to jurisdictional claims in published maps and institutional affiliations.